Biosensors and Bioelectronics 111 (2018) 152–158

Contents lists available at ScienceDirect

Biosensors and Bioelectronics

journal homepage: www.elsevier.com/locate/bios

AuNP-RF sensor: An innovative application of RF technology for sensing pathogens electrically in liquids (SPEL) within the food supply chain

Leann Lerie Matta[a], Saranraj Karuppuswami[b], Premjeet Chahal[b], Evangelyn C. Alocilja[a,*]

[a] Department of Bio systems and Agricultural Engineering, Michigan State University, East Lansing, MI, USA
[b] Department of Electrical and Computer Engineering, Michigan State University, East Lansing, MI, USA

ARTICLE INFO

Keywords:
Bio-sensing
Milk
MNP
Passive RF sensor tag
Threshold detector

ABSTRACT

Rapid detection techniques of pathogenic bacteria in the liquid food supply chain are of significant research interest due to their pivotal role in preventing foodborne outbreaks, and in maintaining high standards of public health and safety. Milk and dairy products are of particular interest due to their widespread consumption across the globe. In this paper, a biosensor for detecting pathogenic bacteria in milk using dextrin-capped gold nanoparticles (d-AuNP) as labels decoded at microwave frequencies is presented. The SPEL (sensing pathogens electrically in liquids) biosensor consists of a 3D printed vial and uses an RF reader and an RFID (radio-frequency identification) compatible Split Ring Resonator (SRR) based tag. The SPEL biosensor is capable of detecting bacteria at 5 log CFU/mL within 75 min, with the possibility of testing multiple concurrent samples. Detection is based on impedance loading of SRR by d-AuNP bound to pathogenic bacteria. Spectrophotometry, along with carbohydrate-functionalized magnetic nanoparticle (MNP) cell capture, is used to verify the sensitivity of the SPEL biosensor with respect to d-AuNP presence. The proof-of-concept device, along with challenges and opportunities for commercialization, are also outlined.

1. Introduction

Milk is a rich, complex liquid, packed with proteins, carbohydrates and fats suspended within a whey matrix, providing vital nutrients to humans, and to opportunistic microbial pathogens (Silanikove et al., 2006). The U.S. is the largest producer of cow's milk in the world, at 196 billion pounds in 2011 (Schultz and Geisler, 2012). Both raw and pasteurized milk products are consumed in the U.S., even though raw milk was involved in 60% of dairy associated foodborne outbreaks in 2006 (Langer et al., 2012). The Food and Drug Administration (FDA) cautions against drinking raw milk and unpasteurized products, due to the severity of diseases that may be contracted from over 90 microbial pathogens that may be present, such as *E. coli*, *Salmonella*, *Streptococcus*, *Staphylococcus*, and *Listeria* (Deperrois-Lafarge and Meheut, 2012). In 2005 – 2006, 80% of children (2 – 11 years) consumed milk (Sebastian et al., 2010), but they are especially susceptible to infections. Pasteurized milk products are safer for human consumption, given they are not cross-contaminated post-sterilization, as occurred in numerous foodborne outbreaks between 1976 and 2007 (FDA, 2011). To protect this valuable commodity and its consumers, farmers and producers alike require rapid, frequent, and reliable testing of milk quality and contamination.

Rapid detection methods in the food supply industry range in their level of specificity and sensitivity to microbial contamination, actual sample processing time, and level of technical difficulty in performing the assay on-site. Due to the perishable nature of milk, the bacterial load in raw milk should be detected in real-time, while pasteurized liquid products should also be tested to ensure the bacterial load is below regulated levels. The FDA has approved culture methods for pathogen detection, but they are time-consuming, labor-intensive, supply-intensive and definitive results are available only after days of incubated bacterial growth (FDA, 2003).

Flow cytometry methods have also been proposed, and is one of the few rapid methods thus-far suggested by the FDA to quantify bacterial presence in milk (Gunasekera et al., 2000). The bench scale system BactoScan FC™ (Foss Electric, Hillerod, Denmark), uses flow cytometry, with fluorescent labeling, and RFID technology for sample identification (Ramsahoi et al., 2011). Flow cytometry methods, in general, are beset with limitations including variable fluorescent cell labeling, flow channels and tips that plug, background lighting interference, and require stringent flushes between samples (Hoffman, 2008). In contrast, methods that can detect cells using inexpensive, prepackaged vials, such as the user-friendly SPEL biosensor concept, provide minimal liquid handling, without the need for repeated system calibration, and

* Corresponding author.
E-mail address: alocilja@msu.edu (E.C. Alocilja).

https://doi.org/10.1016/j.bios.2018.04.010
Received 31 January 2018; Received in revised form 20 March 2018; Accepted 6 April 2018
Available online 11 April 2018
0956-5663/

easy clean-up. A major benefit of our system is that future applications will use RF sensor tags directly for bio-sensing samples which will be easily compatible to existing RFID infrastructure.

Gold nanoparticles (AuNP) find numerous uses in microbiological areas, from medical diagnostic applications to detecting pathogens for food and environmental safety (Dykman and Khlebtsov, 2011; Vetrone et al., 2012; Wang and Alocilja, 2015). Capping agents such as citrate or dextrin provide AuNP stability against electrostatic forces in solution, reducing aggregation, and provide support for subsequent functionalization with various ligands such as DNA, antibodies, or microbiological components (Alkilany and Murphy, 2010; Wang and Alocilja, 2015). Although applications using unmodified dextin-capped nanoparticles of carbon, selenium, and silver have been developed (Afshinnia et al., 2017; Hua et al., 2013; Malhotra et al., 2016), and dextrin-stabilized gold colloids (Porta, 2003), none of these applications use dextrin-capped AuNP (d-AuNP) with RF sensing.

Battery free, long-range passive RF sensing is an important technology for applications involving tracking and tracing along the supply chain (Saranraj Karuppuswami et al., 2016a, 2016b; Want, 2006). The wireless RF tag, coupled with sensing, provides a higher degree of security in quality control along the food supply chain (Karuppuswami et al., 2017,2016a, 2016b). Implantable RF tags have been commonly used for animal tracking (Want, 2006) and also for monitoring the biological environment around stents in human beings (Occhiuzzi et al., 2012). RF tags have also been adapted for label free identification of different biomarkers such as antibodies and nanoparticles (Yuan et al., 2014).

In literature, SRR-based biosensors were developed for detection of biomolecules such as prostate cancer markers, prostate specific antigen and cortisol stress hormone (Chen et al., 2012; Lee et al., 2012). SRR's were also used for sensing the binding of biotin and streptavidin on the sensor surface (Lee and Yook, 2008). A plasmonic SRR has been demonstrated for DNA sensing in the optical regime (Clark et al., 2009). SRR has unique properties such as high quality (Q) factor making it an ideal choice for sensing smaller changes in material properties (Chen et al., 2012).

Using emerging RF bio-sensing technology, the SPEL biosensor presented here combines cell capture inside a plastic well with an SRR-based tag to detect d-AuNP labeling of bacteria as a threshold detector. This design has been proven to allow accurate and rapid detection of bacterial cells in contaminated milk with minimal testing steps, reduced liquid handling and results within 75 min. The sensor is intended to be field deployable for quality control of milk from the farm to the processor. This proof-of-concept SPEL biosensor rapidly detects d-AuNP bound to bacteria within a milk matrix by monitoring the resonance frequency shift due to impedance loading of the SRR. This biosensor uses sample sizes of 20 µL to detect a bacterial load of 5 log CFU/mL by correlating the frequency shift to the number of bound d-AuNP. This biosensor is non-selective and detects total bacterial load. For this proof-of-concept study, *E. coli* C3000 presence in Vitamin D milk was used as the model system. A schematic of the proof-of-concept is shown in Scheme 1.

2. Experimental methods and materials

2.1. E. coli C3000 culture

E. coli C3000 strain was obtained from the Nano-Biosensors Lab at Michigan State University and used as model microbial cells throughout all testing. The colonies from frozen (−70 °C) culture were grown on tryptic soy agar (TSA). A single colony was isolated, inoculated into tryptic soy broth (TSB, Sigma-Aldrich, St. Louis, MO) and grown overnight at 37 °C. One milliliter (mL) of the liquid culture was transferred to a new tube of TSB (9 mL) and incubated at 37 °C for 4 h before each experiment. Tenfold serial dilutions of the bacterial culture, from 10^{-} to 10^{6} colony forming units per milliliter (CFU/mL), were prepared using phosphate buffered saline (PBS, pH 7.4, Neogen, Lansing, MI) before each experiment. Separate similar tenfold dilutions were made in Vitamin D milk (purchased from local commercial seller) from 10^{-} to 10^{10} CFU/mL. Culture diluted in PBS and milk was plated on CHROMagar™ *E. coli* (DRG International, Springfield, NJ), incubated overnight at 37 °C, and enumerated to determine cellular concentration.

2.2. Concentrated gold nanoparticles

Dextrin-capped gold nanoparticles (used as received from the Nano-Biosensors Lab, (Anderson et al., 2011)) were analyzed for their ability to provide sufficient frequency shifts at various concentrations. Excess dextrin in the d-AuNP solution was removed to increase signaling. Concentrated d-AuNP was prepared by removing excess dextrin and solution. Volumes ranging between 25 and 250 µL of the original d-AuNP suspension were transferred to 2 mL pinched-tip centrifuge tubes, sonicated for 10 min, and centrifuged at 15,000 rpm at 4 °C for 20 min. Following supernatant removal, the remaining 20 µL d-AuNP pellet was sonicated for 15 min to evenly distribute the concentrated d-AuNP evenly, then used as the starting aliquot. Even distribution of the concentrated d-AuNP was assured using spectrophotometric scans (900 − 200 nm wavelength, Shimadzu UV-3101PC, UVProbe software, 1000 µL PBS reference) compared to non-concentrated d-AuNP standards of the same original volume, showing peak values at 520 nm for both and no evidence of particle aggregation. Tubes were stored at 4 °C, and used within 24 h of preparation. Concentrated d-AuNP are referred to using their initial volume, e.g. a 75 µL concentrated d-AuNP will be identified as “d-AuNP75”.

2.3. SPEL biosensor material and design

Low-cost 3D (3-dimensional) printing was selected as an economical method for potential large-scale production of SPEL biosensors. After design optimization, the final forms consisted of two wells (~20 µL, one sample and one reference) printed (Stratasys Object Connex350 printer) using VeroWhitePlus (acrylic polymer with free surface electrons). The printer uses a polyjet process where the build material is added as layers in a liquid form and then selectively cured with ultra-violet light. The schematic of the SPEL biosensor and dimensions are shown in Fig. 1.

2.4. Split-ring resonator design

SRR designed in this paper consists of two square split rings capacitively coupled to a transmission line, one used for measurement and the other for reference. The SRR is designed using ANSYS HFSS®; and fabricated by conventional photo lithography and etching, using Roger's 3003 laminates (thickness ~1.52 mm). The SRR is measured using a Vector network analyzer (VNA) and the resonance frequency of the first ring was at 3.4 GHz and second at 4.8 GHz. Since the first ring has higher Q-factor than the second one, it was chosen as the measurement ring for all experiments. The schematic of the developed SRR sensor along with the dimensions, measured scattering (S) parameters and electric field (E-field) distribution at the resonance frequency (3.4 GHz), are shown in Fig. 2. The crucial element for detecting a small change in the number of d-AuNP present is to create strong electric fields in the gap region of the SRR sensor. The d-AuNP perturb the E-field in the gap region and thereby shift the resonance frequency of the SRR.

2.5. Culture verification of cell attachment to SPEL biosensor in the presence of milk

Single-well SPEL biosensors were filled with 20 µL of milk spiked with cells at 3, 5 and 7 log CFU/mL. Cells were incubated for 30 min, then unattached cells rinsed with 500 µL PBS. Concentrated d-AuNP25

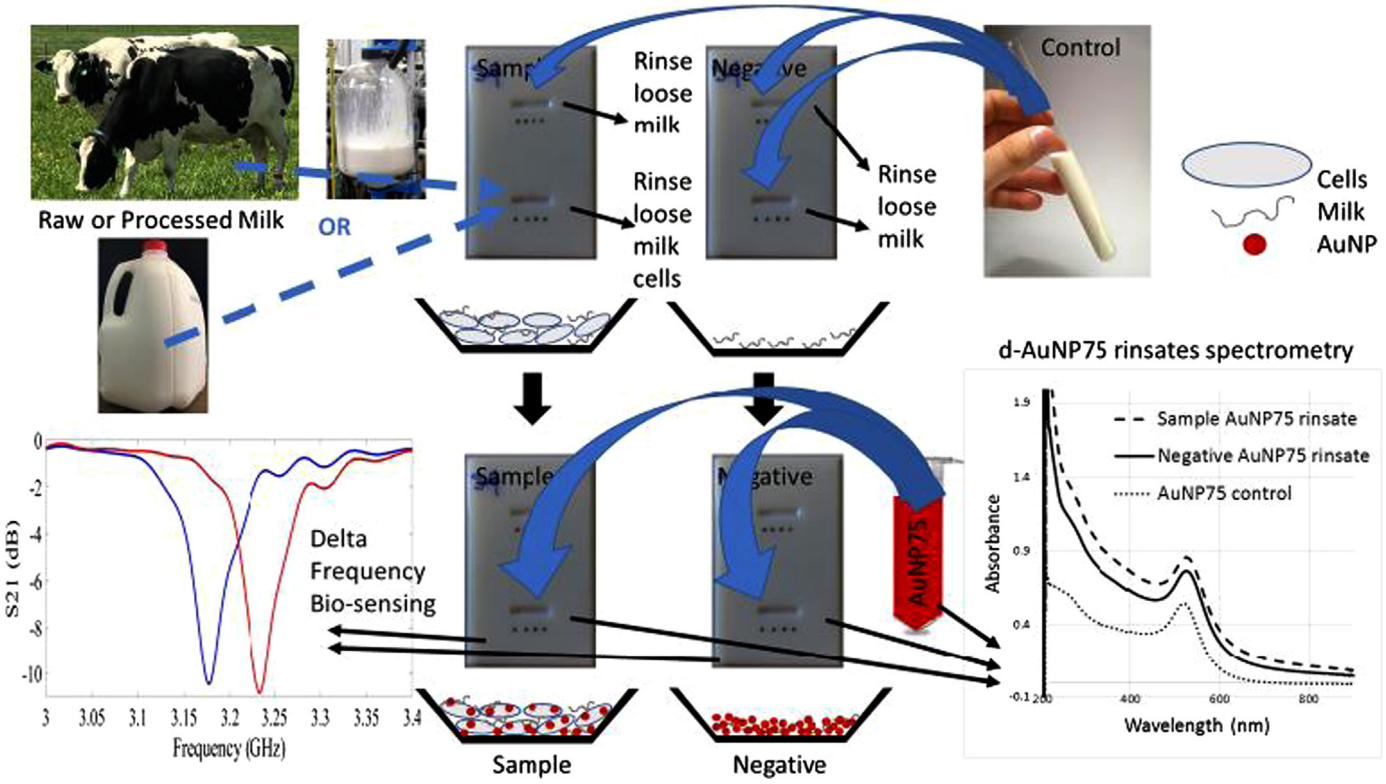

Scheme 1. *Schematic of the SPEL biosensor for total bacterial load.* Artificially contaminated milk is applied to the bottom Sample well (left) while sterile milk is applied to the bottom Negative control well (right) as well as both top wells (left & right). Cells and milk attach for 30 min, then rinsed with PBS to remove unattached milk and cells. Concentrated d-AuNP was applied to the bottom Sample and Negative control wells to attach for 30 min, then rinsed with PBS. RF frequency shifts were read for all 4 wells (left) to determine cell concentration and spectrophotometric absorbance of the d-AuNP rinsates confirmed RF signaling trends (right).

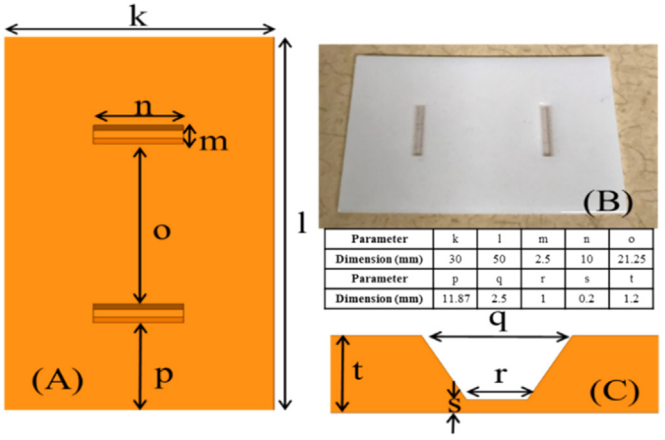

Fig. 1. Design of the SPEL biosensor (A, top view, and C side view), and optical image (B), along with its dimensions.

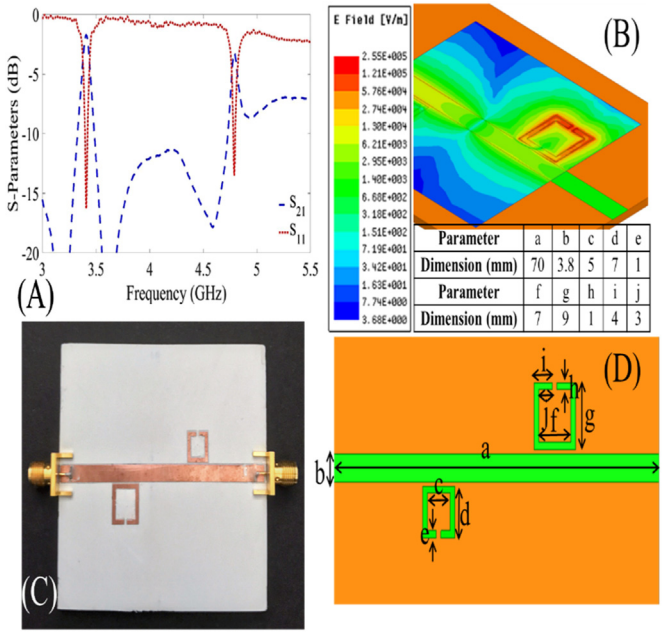

Fig. 2. Measured S-Parameters (A), E-Field distribution at the resonance frequency (B), image of the SRR (C), schematic of the designed SRR (D) and a table listing its dimensions.

was applied to the wells and incubated for 30 min, then rinsed with 500 µL PBS. Both rinsates were combined onto sterile petri dishes and cultured with CHROMagar. The SPEL biosensors were then submerged into 15 mL TSB in a 50 mL Eppendorf tube and rotated at 100 rpm overnight. A 100 µL sample from each culture tube were plated on CHROMagar. All cultures were incubated overnight at 37 °C. Negative controls were prepared same as samples but without cells, and all samples and controls were run in triplicate.

2.6. Spectrophotometric verification of d-AuNP signaling with milk matrix effects

Correlation between d-AuNP quantity and frequency shift was determined for concentrated amounts of d-AuNP between 25 µL and 100 µL in steps of 25uL in the presence of milk. All wells of the SPEL biosensors were initially exposed to 20 µL of milk for 30 min, then rinsed with 500 µL of PBS. Concentrated d-AuNP were then applied to only the bottom well of each form and allowed to dry (n = 3). These

forms were then tested for frequency shift. The same concentrated d-AuNP volumes were diluted in PBS to 1 mL and spectrophotometric scans were run from 900 nm to 200 nm wavelength (n = 3). The resulting integrated spectral absorbance was calculated using numerical step integration between 220 and 900 nm. Linear regression was used to determine the relationships between frequency shift and d-AuNP volume, and spectral area and d-AuNP volume.

2.7. Spectrophotometric confirmation of d-AuNP attachment following cell capture

MNP (carbohydrate-functionalized MNP, developed in the Nanobiosensors Lab, (Wang and Alocilja, 2015)) was used as a SPEL biosensor substitute to study d-AuNP attachment to cells with spectrometry. These MNP are proven in-lab to capture microbial cells within a complex milk matrix at over 70% (log CFU/mL basis). MNP (20 µL of 5 mg/mL) were exposed to 20 µL of 5 log CFU/mL cell culture plus 100 µL PBS for 5 min, magnetically separated and re-suspended within d-AuNP250 plus 40 µL PBS. d-AuNP250 attachment was allowed for 10, 20 and 30 min incubation times. The "MNP-cell-AuNP" complexes were re-suspended within 1000 µL PBS. Negative controls followed the same procedure except without cells. Spectral absorbance was measured between 900 nm and 200 nm wavelength. Peak absorbances for MNP (620 nm) and d-AuNP (520 nm) were monitored. All spectra were numerically step-integrated between 900 and 220 nm for MNP-cell-AuNP complexes and negative controls (n = 3). This same method was subsequently used with cells suspended in milk, except d- AuNP250 attachment times were for only 30 min (n = 3).

2.8. Cell signaling using frequency shifts of d-AuNP labeling

Cells grown to log phase within TSB were diluted to approximately 5 log CFU/mL within milk. SPEL biosensors similar to the one shown in Fig. 2B were used for RF bio-sensing, with the upper wells acting as the references, and the lower wells used for samples or negative controls. Milk (20 µL) was allowed to attach for 30 min to reference wells, followed by rinsing with 500 µL PBS. This step is to provide reference for the effects of milk residue and plastic anomalies in samples and negative controls. Samples were prepared using 20 µL of diluted cell culture and allowed to attach for 30 min, followed by a 500 µL PBS rinse. Then, d-AuNP75 was applied and allowed to attach for 30 min, followed by a 500 µL PBS rinse. Negative controls followed the above procedure, but without cells. All samples and negative controls were tested for frequency shift along the well, normalized with respect to their reference well, and the values averaged per form (n = 3).

3. Results and discussion

3.1. RF signaling of E. coli contamination with culture and SEM imaging verification

A proof-of-concept SPEL (sensing pathogens electrically in liquids) biosensor for broad bacterial detection in contaminated milk was designed and analyzed. This biosensor uses non-selective cell capture and d-AuNP labeling with an emerging SRR-based RF bio-sensing approach to detect the numerous pathogens at environmental levels that may contaminate dairy and water resources. RF frequency shift results (Fig. 3A) show significantly lower responses for samples with approximately 5.1 log CFU/mL *E. coli* C3000 ("SPEL-cell-AuNP"), clearly discriminating against higher negative control levels ("SPEL-AuNP") (n = 6). The inverse signaling relationship is the result of less d-AuNP present in the samples causing a lower shift in the RF frequency.

Cell attachment to the SPEL biosensor reduces available area for d-AuNP binding, causing decreased RF frequency shifts for samples. *E. coli* C3000 adherence was verified by separately culturing both unattached cells and captured cells. On average, unattached cells numbered fewer than 3 log CFU, 100 CFU and 25 CFU for capture of 7, 5 and 3 log CFU/mL contaminated milk, respectively. Attached cells were labeled with d-AuNP, then SPEL biosensors were cultured in TSB, followed by solid agar. Resulting cultured SPEL-cell-AuNP plate counts were too high for enumeration, proving cell attachment to the SPEL biosensor and biocompatibility of d-AuNP labeling to the cells. Meanwhile negative control SPEL biosensor culturing showed no cell growth.

Scanning electron microscopy (SEM) (JEOL 7500 F, JEOL Ltd. Tokyo, Japan) further confirmed cell attachment, as well as d-AuNP attachment, to the SPEL biosensors. An example of the 2-well SPEL biosensor for cell capture and d-AuNP labeling is shown in Fig. 1B. Cells appeared to bind in single layers (Fig. S1B). Subsequent d-AuNP binding to the cell surface (Fig. 3B) is seemingly selective and at lower concentrations than to the SPEL biosensor itself (Fig. 3C), where arrows point to d-AuNP groupings, identified with low-angle background emission SEM. Reduced d-AuNP presence, due to cell crowding and selective cell surface binding, results in lower RF frequency shifts for samples.

3.2. TEM imaging of d-AuNP attachment to E. coli cells

Transmission electron microscopy (TEM, JEOL 100 ×, MSU) was used to corroborate MNP as a substitute cell support of the SPEL biosensor, and to verify key aspects of d-AuNP attachment to *E. coli* C3000 cells. MNP (200 nm diameter) rapidly extract *E. coli* C3000 cells from contaminated milk as MNP-cell complexes. These complexes were then labeled with concentrated d-AuNP ("MNP-cell-AuNP"). TEM images showed that d-AuNP (5 – 15 nm diameter, Fig. 4A) bind to cells in aggregated groupings of less than 50 nm wide dispersed along the cell wall (Fig. 4B), but not to flagella, even for cells in milk. This seemingly selective binding duplicates the binding seen in SEM images (Fig. 3B). This reduced d-AuNP presence contrasts with saturation binding to MNP without cells present ("MNP-AuNP") in PBS (Fig. 4C), or even milk (Fig. S2), duplicating the d-AuNP binding to SPEL biosensors seen in SEM (Fig. 3C).

3.3. Spectrophotometric verification of d-AuNP RF frequency shift signaling

Spectrophotometric measurements of MNP-based complex absorbance was used to verify RF frequency shifts for various SPEL biosensor d-AuNP labeling conditions. Spectra for concentrated d-AuNP prepared for RF signaling have sharp peaks at 520 nm, indicating that sufficient dextrin capping was retained around the gold nanoparticles to prevent aggregation (Fig. S3A). Peaks for 75 µL unconcentrated and unconcentrated d-AuNP are also the same, indicating no loss in d-AuNP quantity during concentration. RF frequency shifts of 13–47 MHz for SPEL biosensors containing these same dried standards showed a linear relationship to the initial d-AuNP volumetric amount (n = 12, R^2 = 0.97, Fig. 5A). Integrated spectrum absorbance between 220 and 900 nm for the concentrated d-AuNP standards also showed a strong linear relationship to the initial d-AuNP volume (n = 12, R^2 = 0.99, Fig. 5A).

MNP capture of *E. coli* C3000 cells for MNP-cell-AuNP standard preparation simulated SPEL-cell-AuNP complexes, and their absorbance was quantified with spectrophotometry. Peak absorbances for MNP (620 nm) and d-AuNP250 (520 nm) standards, show an additive spectral effect in a combined mixture(Fig. S3B). Similarly, spectrum of standards prepared by d-AuNP250 timed exposure to MNP-cell complexes showed linearly increasing AuNP absorbance peak heights, and therefore attachment, with time (R^2 = 0.99, Fig. S3C). In addition, over 10% more d-AuNP attached to free MNP as MNP-AuNP, like saturated SPEL-AuNP binding. Since MNP-cell-AuNP spectrum for samples become convoluted, due to the additive effect of component peaks (Fig. 5B), standards spectra were also numerically step-integrated between 220 and 900 nm. These integrated spectra also showed linear increases in d-AuNP binding with time (R^2 = 0.99, Fig. 5C).

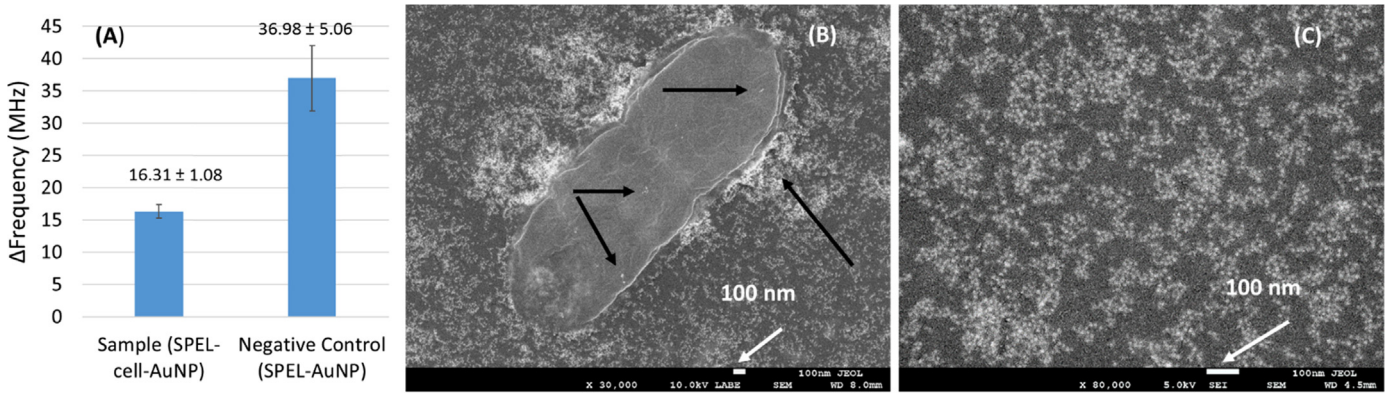

Fig. 3. RF frequency shifts for E. coli bio-sensing and SEM imaging. RF frequency shifts for samples with 5.1 log CFU/mL (SPEL-cell-AuNP) versus negative controls without cells (SPEL-AuNP) (n = 6) (A). Cell attached to SPEL biosensor with selective d-AuNP75 attachment to the cells and higher attachment to the SPEL biosensor (see arrows) (SPEL-cell-AuNP) (B), and saturating d-AuNP75 attachment to the SPEL biosensor (SPEL-AuNP) (C). RF = radio frequency, SPEL = sensing pathogens electrically in liquids, d-AuNP75 = 75 µL concentrated dextin-capped gold nanoparticles, SEM = scanning electron microscopy.

MNP-cell-AuNP spectrum for capture within contaminated milk samples were more convoluted (Fig. 5B) than standards (Fig. S3B), making spectrum integration a necessary tool for spectral analysis. Also, a reduction in absorbance for samples compared to standards was seen due to the loss of MNP residue and unbound d-AuNP75, and a shift in the AuNP peak to approximately 535 nm. Again, absorbance was higher for negative control MNP-AuNP complexes than for sample MNP-cell-AuNP complexes, due to selective d-AuNP-cell binding. This same inverted signaling response mimics SPEL biosensor RF frequency shifts.

3.4. Binding mechanisms between cells, SPEL biosensor, MNP and d-AuNP

Both bio-sensing samples, SPEL-cell-AuNP RF frequency shifts and MNP-cell-AuNP integrated spectral absorbance, showed lower values than their respective negative controls. This inverted signaling is explained through electrostatic binding of *E. coli* C3000 cells to SPEL biosensors, MNP and d-AuNP. Cell surfaces contain numerous molecular structures composed of sugar, lipid and amino acid moieties. Microbes use these structures to bind to surfaces and uptake nutrients. SPEL biosensor VeroWhitePlus acrylic surfaces are hydrophobic, and *E. coli*, within only 10 s, adhered stronger and faster to hydrophobic fluorosilane surfaces (Xu et al., 2013). During capture from milk, cells create hydrophobic bonds to the acrylic surface, while displacing milk constituents (fats, proteins and carbohydrates) and water. Negatively-charged dextrin hydroxyl groups binding to positively charged amino acids describes both selective d-AuNP-cell binding through specific cell surface polypeptides (Figs. 3B and 4B) versus saturation of the MNP-carbohydrate amino groups (Fig. 4C and Fig. S2). Meanwhile, d-AuNP-SPEL binding involves displacement of the AuNP dextrin cap through repulsion of its hydroxyl group by the acrylic electron-rich oxygen atoms. The exposed, positively- charged AuNP surface then ionically saturates the abundance of acrylic oxygen atoms (Fig. 3C). These binding dynamics result in reduced d-AuNP labeling for samples on either the SPEL biosensors or MNP surfaces due to both selective d-AuNP cell binding and cell presence impeding d-AuNP access to the support surface, whereas non-cell negative controls have higher binding, resulting in the inverted signaling.

One concern in working with nanoparticles is their aggregation, which would reduce their ligand binding efficiency. SEM (Fig. 3B - C) and TEM (Fig. 4A – C, and Fig. S2) imaging verified that throughout both the d-AuNP processing and testing steps, they did not aggregate in the presence of PBS nor milk components. This ensured the full binding capacity of the d-AuNP. In addition, Fig. 4B does clearly show selective binding of d-AuNP to cell surface molecules in aggregates of approximately 50 nm. Polypeptides on cell surfaces contain pockets of positively charged amino acids, which seemingly attracted multiple d-AuNP.

3.5. Reproducibility, stability and specificity of the SPEL biosensor

To determine reproducibility of the proof-of-concept biosensor at the applied cell concentration, two experiments with 3 replicates each

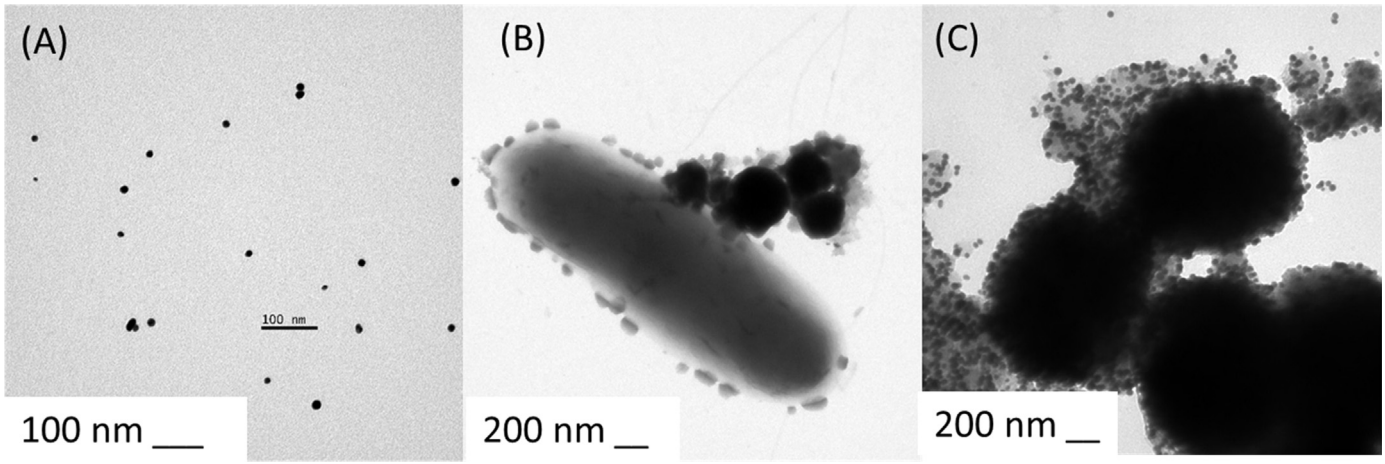

Fig. 4. TEM images of d-AuNP attachment to E. coli cells and MNP. d-AuNP alone (A), attached to MNP-cell complexes (B), and attached to MNP in PBS matrix (C). d-AuNP = dextrin-capped gold nanoparticles, MNP = magnetic nanoparticles, PBS = phosphate buffered saline.

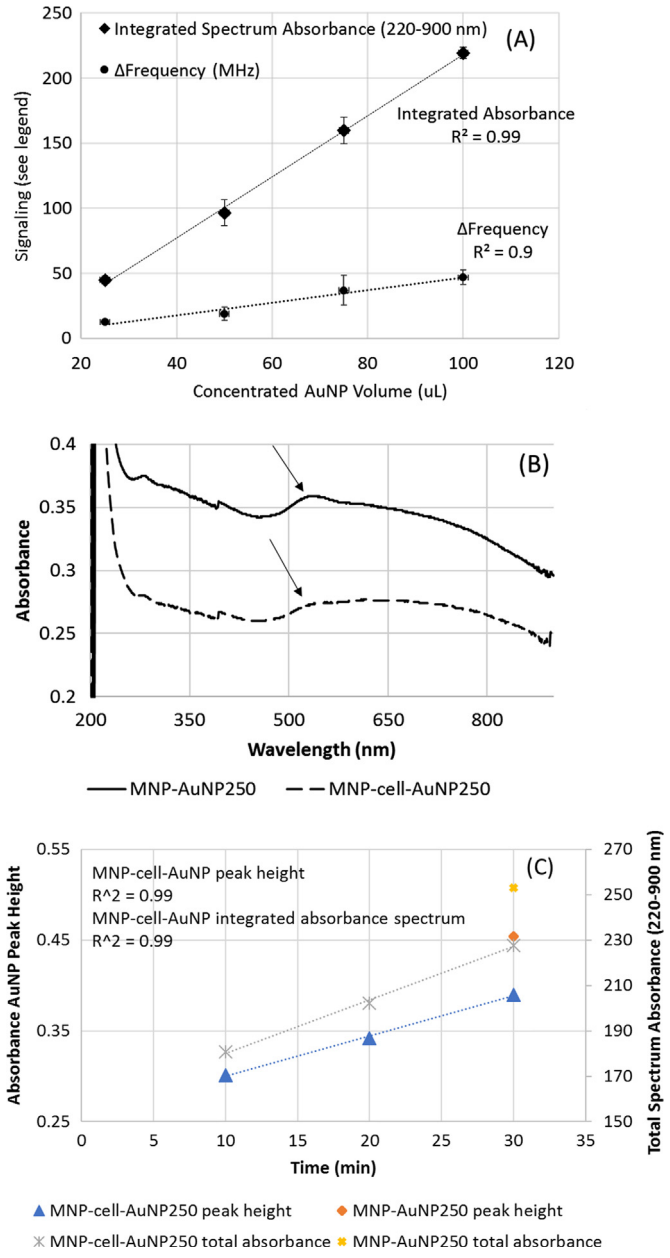

Fig. 5. *Spectrophotometric measurement of d-AuNP presence.* Frequency shifts and integrated spectrum absorption for concentrated d-AuNP volumes (A). MNP capture of E. coli cells in milk and d-AuNP250 attachment, with arrows indicating the AuNP peak at approximately 520 nm (B). Comparison of AuNP absorbance peak height (520 nm) and integrated spectrum absorbance between 220 and 900 nm for d-AuNP250 timed attachment (C). All controls were run in triplicate, their values averaged, and standard deviation calculated. d-AuNP250 = 250 µL of d-AuNP concentrated to approximately 20 µL by centrifugation and removal of excess supernatant, MNP = magnetic nanoparticles.

(n = 6) were prepared independently on separate days (to remove environmental bias) and tested for frequency shift due to d-AuNP labeling. Frequency shifts were 15.42 ± 0.68 and 17.21 ± 0.14 for cell concentrations of 1.36×10^4 CFU/mL and 2.58×10^5 CFU/mL, respectively. These values were averaged to give the reported results shown in Fig. 3A.

The economical design of the d-AuNP and SPEL biosensor allowed it to be disposable, eliminating concerns of false signaling responses from previous tests. Given the expedited time for detection, though, it is foreseeable that attached cells and d-AuNP could be removed using a PBS rinse. Still, the stability of the biosensor form would need to be evaluated in the future if repeated used was desired.

Due both to the dextrin carbohydrate ligand and lack of functionality in the capture well, the economical biosensor described here detects total bacterial load present with specificity to bacteria. It was found that *E. coli* cells selectively bound to the well surface even in the presence of a complex matrix such as milk. Pathogen selectivity could be introduced using antibody to functionalize the well or d-AuNP, but this would increase production and storage costs, while reducing shelf-life. Advances in identifying more selective carbohydrate ligands towards pathogens in our food (Safina et al., 2008; Shi and Yu, 2012; Yazgan et al., 2014), though, show promise in detecting specific targets while keeping costs under control.

4. Conclusions

SPEL biosensor threshold detection of 5 log CFU/mL *E. coli* C3000 contamination in Vitamin D milk is reliable and reproducible, with minimal testing time and steps. The RF bio-sensor described here showed smaller RF frequency shifts from selective d-AuNP attachment to cell samples versus larger frequency shifts from saturated d-AuNP attachment to negative controls. These inverted results were verified using SEM, TEM, and spectrophotometry, which helped to elucidate d-AuNP attachment to cells and supports. Sample MNP-cell-AuNP integrated spectrum absorbance was also introduced and shown to be an accurate measure of sample quantity.

Design enhancements for this proof-of-concept RF bio-sensing technology that would improve usability, lower threshold sensitivity, minimize testing complexity and further reduce sampling time, are: increased sample volume and pre-loaded d-AuNP vials (instead of flat forms), for one-step simultaneous capture and label. This inexpensive AuNP-RF sensor design detects a broad-spectrum total bacterial load due to non-selective cell binding to the SPEL biosensor and d-AuNP. Pathogen specificity is plausible via SPEL biosensor functionalization with selective antibodies, though at increased user costs. Additionally, a wireless biosensor is possible by integrating an antenna to the sensor-tag for compatibility with existing industrial RFID infrastructure to also allow field operability with handheld SPEL biosensor interrogation. Conceivably, low cost, self-contained SPEL biosensor kits could be commercialized for liquid food quality control across the food supply chain.

Acknowledgements

This work was supported by The Axia Institute at Michigan State University.

Appendix A. Supplementary material

Supplementary data associated with this article can be found in the online version at http://dx.doi.org/10.1016/j.bios.2018.04.010.

References

Afshinnia, K., Sikder, M., Cai, B., Baalousha, M., 2017. Effect of nanomaterial and media physicochemical properties on Ag NM aggregation kinetics. J. Colloid Interface Sci. 487, 192–200. http://dx.doi.org/10.1016/j.jcis.2016.10.037.

Alkilany, A.M., Murphy, C.J., 2010. Toxicity and cellular uptake of gold nanoparticles: what we have learned so far? J. Nanopart. Res. 12, 2313–2333. http://dx.doi.org/10.1007/s11051-010-9911-8.

Anderson, M.J., Torres-Chavolla, E., Castro, B.A., Alocilja, E.C., 2011. One step alkaline synthesis of biocompatible gold nanoparticles using dextrin as capping agent. J. Nanopart. Res. 13, 2843–2851. http://dx.doi.org/10.1007/s11051-010-0172-3.

Chen, T., Li, S., Sun, H., 2012. Metamaterials application in sensing. Sensors 12, 2742–2765.

Clark, A.W., Glidle, A., Cumming, D.R., Cooper, J.M., 2009. Plasmonic split-ring resonators as dichroic nanophotonic DNA biosensors. J. Am. Chem. Soc. 131, 17615–17619.

Deperrois-Lafarge, V., Meheut, T., 2012. Use of the rpoB gene as an alternative to the V3 gene for the identification of spoilage and pathogenic bacteria species in milk and

milk products: use of the rpoB gene as an alternative to the V3 gene. Lett. Appl. Microbiol. 55, 99–108. http://dx.doi.org/10.1111/j.1472-765X.2012.03261.x.
Dykman, L.A., Khlebtsov, N.G., 2011. Gold nanoparticles in biology and medicine: recent advances and prospects. Acta Nat. 3, 34–55.
FDA, 2011. Buy, Store & Serve Safe Food: Raw Milk Misconceptions and the Danger of Raw Milk Consumption [WWW Document]. URL 〈https://www.fda.gov/Food/FoodborneIllnessContaminants/BuyStoreServeSafeFood/ucm247991.htm〉 (accessed 21 April 2017).
FDA, 2003. Bacteriological Analytical Manual (BAM) [WWW Document]. URL 〈http://www.fda.gov/Food/FoodScienceResearch/LaboratoryMethods/ucm2006949.htm〉 (accessed 29 October 2015).
Gunasekera, T.S., Attfield, P.V., Veal, D.A., 2000. A flow cytometry method for rapid detection and enumeration of total bacteria in milk. Appl. Environ. Microbiol. 66, 1228–1232. http://dx.doi.org/10.1128/AEM.66.3.1228-1232.2000.
Hoffman, R.A., 2008. Flow cytometry: instrumentation, applications, future trends and limitations. In: Resch-Genger, U. (Ed.), Standardization and Quality Assurance in Fluorescence Measurements II. Springer Berlin Heidelberg, Berlin, Heidelberg, pp. 307–342. http://dx.doi.org/10.1007/4243_2008_037.
Hua, X., Du, Y., Chen, J., Xu, G., Yu, T., Zhang, Q., 2013. Evaluation of the enantioselectivity of carbon nanoparticles-modified chiral separation systems using dextrin as chiral selector by capillary electrokinetic chromatography: CE and CEC. Electrophoresis 34, 1901–1907. http://dx.doi.org/10.1002/elps.201200627.
Karuppuswami, S., Arangali, H., Chahal, P., 2016a. A hybrid electrical-mechanical wireless magnetoelastic sensor for liquid sample measurements, In: Proceedings of the IEEE 66th Electronic Components and Technology Conference (ECTC), pp. 2535–2540. https://doi.org/10.1109/ECTC.2016.283.
Karuppuswami, S., Kaur, A., Arangali, H., Chahal, P.P., 2017. A hybrid magnetoelastic wireless sensor for detection of food adulteration. IEEE Sens. J. 17, 1706–1714.
Karuppuswami, S., Kaur, A., Ghazali, M.I.M., Chahal, P., 2016b. RFID compatible sensor tags for remote liquid sample interrogation. IEEE 2401–2407. http://dx.doi.org/10.1109/ECTC.2016.282.
Langer, A.J., Ayers, T., Grass, J., Lynch, M., Angulo, F.J., Mahon, B.E., 2012. Nonpasteurized dairy products, disease outbreaks, and state laws—United States, 1993–2006. Emerg. Infect. Dis. 18, 385–391. http://dx.doi.org/10.3201/eid1803.111370.
Lee, H.-J., Lee, J.-H., Moon, H.-S., Jang, I.-S., Choi, J.-S., Yook, J.-G., Jung, H.-I., 2012. A planar split-ring resonator-based microwave biosensor for label-free detection of biomolecules. Sens. Actuators B Chem. 169, 26–31.
Lee, H.-J., Yook, J.-G., 2008. Biosensing using split-ring resonators at microwave regime. Appl. Phys. Lett. 92, 254103.
Malhotra, S., Welling, M.N., Mantri, S.B., Desai, K., 2016. *In vitro* and *in vivo* antioxidant, cytotoxic, and anti-chronic inflammatory arthritic effect of selenium nanoparticles: *in vitro* and *in vivo* effect of SeNP. J. Biomed. Mater. Res. B Appl. Biomater. 104, 993–1003. http://dx.doi.org/10.1002/jbm.b.33448.
Occhiuzzi, C., Contri, G., Marrocco, G., 2012. Design of implanted RFID tags for passive sensing of human body: the STENTag. IEEE Trans. Antennas Propag. 60, 3146–3154.
Porta, F., 2003. Gold nanostructured materials for the selective liquid phase catalytic oxidation. J. Mol. Catal. Chem. 204–205, 553–559. http://dx.doi.org/10.1016/S1381-1169(03)00338-8.
Ramsahoi, L., Gao, A., Fabri, M., Odumeru, J.A., 2011. Assessment of the application of an automated electronic milk analyzer for the enumeration of total bacteria in raw goat milk. J. Dairy Sci. 94, 3279–3287. http://dx.doi.org/10.3168/jds.2010-4102.
Safina, G., Vanlier, M., Danielsson, B., 2008. Flow-injection assay of the pathogenic bacteria using lectin-based quartz crystal microbalance biosensor. Talanta 77, 468–472. http://dx.doi.org/10.1016/j.talanta.2008.03.033.
Schultz, M., Geisler, M., 2012. Fluid Milk Profile | Agricultural Marketing Resource Center [WWW Document]. URL 〈http://www.agmrc.org/commodities-products/livestock/dairy/fluid-milk-profile/〉 (accessed 25 April 2017).
Sebastian, R.S., 2010. others. Fluid Milk Consumption in the United States.
Shi, X.-Z., Yu, X.-Q., 2012. The extended loop of the C-terminal carbohydrate-recognition domain of Manduca sexta immulectin-2 is important for ligand binding and functions. Amino Acids 42, 2383–2391. http://dx.doi.org/10.1007/s00726-011-0980-5.
Silanikove, N., Merin, U., Leitner, G., 2006. Physiological role of indigenous milk enzymes: an overview of an evolving picture. Int. Dairy J. 16, 533–545. http://dx.doi.org/10.1016/j.idairyj.2005.08.015.
Vetrone, S.A., Huarng, M.C., Alocilja, E.C., 2012. Detection of non-PCR amplified S. enteritidis genomic DNA from food matrices using a gold-nanoparticle DNA biosensor: a proof-of-concept study. Sensors 12, 10487–10499. http://dx.doi.org/10.3390/s120810487.
Wang, Y., Alocilja, E.C., 2015. Gold nanoparticle-labeled biosensor for rapid and sensitive detection of bacterial pathogens. J. Biol. Eng. 9. http://dx.doi.org/10.1186/s13036-015-0014-z.
Want, R., 2006. An introduction to RFID technology. IEEE Pervasive Comput. 5, 25–33.
Xu, H., Murdaugh, A.E., Chen, W., Aidala, K.E., Ferguson, M.A., Spain, E.M., Núñez, M.E., 2013. Characterizing pilus-mediated adhesion of biofilm-forming *E. coli* to chemically diverse surfaces using atomic force microscopy. Langmuir 29, 3000–3011. http://dx.doi.org/10.1021/la304745s.
Yazgan, I., Noah, N.M., Toure, O., Zhang, S., Sadik, O.A., 2014. Biosensor for selective detection of E. coli in spinach using the strong affinity of derivatized mannose with fimbrial lectin. Biosens. Bioelectron. 61, 266–273. http://dx.doi.org/10.1016/j.bios.2014.05.008.
Yuan, M., Alocilja, E.C., Chakrabartty, S., 2014. A novel biosensor based on silver-enhanced self-assembled radio-frequency antennas. IEEE Sens. J. 14, 941–942. http://dx.doi.org/10.1109/JSEN.2013.2296155.